A Comparison of Corona-Treated and Flame-Treated Polypropylene Films

Mark Strobel,[1,5] **Viv Jones,**[1] **Christopher S. Lyons,**[1]
Michael Ulsh,[1] **Mark J. Kushner,**[2] **Rajesh Dorai,**[3]
and Melvyn C. Branch[4]

The comparison of corona-treated and flame-treated polypropylene (PP) films provides insight into the mechanism of these surface-oxidation processes. Atomic force microscopy (AFM), contact-angle measurements, and X-ray photoelectron spectroscopy (XPS or ESCA) were used to characterize surface-treated biaxially oriented PP. While both processes oxidize the PP surface, corona treatment leads to the formation of water-soluble low-molecular-weight oxidized materials (LMWOM), while flame treatment does not. Computational modeling of the gas-phase chemistry in an air corona was performed using a zero-dimensional plasma-chemistry model. The modeling results indicate that the ratio of O to OH is much higher in a corona discharge than in a flame. Chain scission and the formation of LMWOM are associated with reactions involving O atoms. The higher ratios of O to OH in a corona are more conducive to LMWOM production. Surface-oxidized PP exhibits considerable thermodynamic contact-angle hysteresis that is primarily caused by microscopic chemical heterogeneity.

KEY WORDS: corona surface modification; flame surface modification; atomic force microscopy; electrical discharges; contact-angle measurements; low-molecular-weight oxidized materials.

1. INTRODUCTION

Polypropylene (PP) films generally require some type of surface modification prior to commercial use. Surface oxidation is the most common modification performed to PP. Oxidized PP surfaces tend to have improved wetting and adhesion properties when compared with the unmodified polymer. In industry, the two

[1] 3M Company, 3M Center, St. Paul, Minnesota.
[2] Department of Electrical and Computer Engineering, University of Illinois, Urbana, Illinois.
[3] Department of Chemical Engineering, University of Illinois, Urbana, Illinois.
[4] Department of Mechanical Engineering, Center for Combustion and Environmental Research, University of Colorado, Boulder, Colorado.
[5] To whom correspondence should be addressed at 3M Company, 3M Center, Building 208-1-01, St. Paul, Minnesota 55144-1000; e-mail: mastrobel1@mmm.com.

processes most widely used to oxidize PP are corona discharges and flame. Although both processes oxidize a thin surface region of the PP, there are significant differences between the surfaces generated by the two techniques. In an earlier paper,[1] we compared corona discharge, flame, air plasma, ozone, and combined UV/ozone (UVO) treatments. That work focused on the extent and depth of oxidation. In this work, we use atomic force microscopy (AFM), X-ray photoelectron spectroscopy (XPS or ESCA), and contact-angle measurements to investigate the surface properties of PP modified by corona and flame processes. The detailed comparison of corona and flame treatments leads to further insights into the mechanism of these important surface-oxidation processes.

Although difficult to investigate directly, "surface molecular weight" has a critical role in determining the wettability, adhesion properties, and permanence (aging behavior) of surface-modified polymers. In our opinion, surface molecular weight is comparably important in the determination of practical performance properties as the extent of oxidation and the types of oxidized functionalities found on a modified polymer.

In the past,[2–4] we tried to investigate surface molecular weight through the detection of water-soluble low-molecular-weight oxidized material (LMWOM). The presence of LMWOM on polymers can be detected by a number of analytical techniques performed in conjunction with washing of the treated surface. LMWOM is characteristically soluble in "polar" solvents such as water, alcohols, and ketones, but remains insoluble in nonpolar solvents such as the alkanes and aromatics.

More recently, we used AFM[5] to directly examine the surface topography of flame-treated PP. We found that flame treatment creates a "nodular" surface topography that is caused by the oxidation of the PP rather than by any heating of the PP surface that might occur in the flame. The surface topography, wettability, and extent of oxidation of flame-treated PP were not affected by washing with any type of solvent, so we concluded that no water-soluble LMWOM was formed. We believe that the nodular topography of flame-treated PP is formed by the agglomeration and rearrangement of intermediate-molecular-weight oxidized products.

Our recent study of flame surface treatments[5] benefited from the use of the SPIN computational model to examine the gas-phase chemistry of impinging flames. The identification and quantification of the gas-phase species in the flame yielded a number of unexpected insights into the mechanism of flame treatment. A computational model that provides similarly detailed gas-phase information for the type of discharge used in industrial corona treating has not been previously available. In this study, we present our first results from the computational modeling of an industrial corona-treating system. The use of this new model helps to explain a number of the characteristics of corona-treated PP.

The nomenclature of atmospheric-pressure electrical discharges can be somewhat confusing. The widely used process for polymer surface modification has long been termed a "corona discharge." However, because of the presence of a dielectric

material on at least one of the discharge electrodes, industrial corona discharges are more properly termed "alternating-current, atmospheric-pressure dielectric-barrier discharges." In this paper, we retain the historic "corona" terminology that is still overwhelmingly used in the polymer industry.

2. EXPERIMENTAL

2.1. Corona and Flame Treatments

Biaxially oriented 30-cm wide isotactic PP film was the substrate used in this study. The 0.05-mm thick PP film was produced using a homopolymer resin with a weight-average molecular weight of 3.6×10^5, a polydispersity index of 4.0, and a peak melting temperature of $163°C$. The base resin contained ca. 200 ppm of an inorganic acid scavenger and ca. 1000 ppm of high-molecular-weight phenolic antioxidants. The additives are not detectable by either ESCA or time-of-flight static secondary ion mass spectrometry (SSIMS). This is the same clean, well-characterized commodity PP film that we have used in studies dating back to the late 1980s.

Corona treatment was performed using industrial equipment manufactured by Pillar Technologies (Hartland, WI). During treatment, the PP film was in contact with a 25-cm diameter, 50-cm face-width steel ground roll coated with a 2.0-mm thick layer of American Roller (Union Grove, WI) # CL500 ceramic dielectric. In this so-called "covered-roll" electrode configuration, the powered electrode consisted of two 200 cm^2, 33-cm face-width stainless steel "shoes" separated from the ground roll by an electrode gap of 1.5 mm. The treater housing was continually flushed with ca. 5000 cm^3/s of either dried or humidified air at 25°C to maintain relative humidities in the discharge region of either 2–5% or 95–100%.

The net power dissipated in the corona was measured with the power meter incorporated into the Pillar P1000 (3.5 kW) power supply. The power meter was carefully calibrated using voltage–charge parallelograms (Lissajous figures), a method first described by Manley[6] and refined by the manufacturers of industrial corona equipment. (C. R. Ballard, Pillar Technologies, Hartland, WI, personal communication, 1988 and 1993). The discharge frequency was 9.6 kHz. The normalized energy of the corona treatment was calculated from the net power and the film speed:

$$\text{Normalized energy, } E = P/ws$$

where P is the net power (in W), w is the electrode face width (in cm), and s is the film speed (in cm/s). Typical units are J/cm^2. To obtain a range of surface oxidation on the PP, we varied the corona energy from 0.1 to 17 J/cm^2 by using film speeds from 1 to 150 m/min at powers from 300 to 2000 W. At a given normalized energy, all combinations of corona power and film speed yielded similar results.

Flame treaters ordinarily employ laminar-premixed flames in which the fuel and the oxidizer are thoroughly mixed prior to combustion. In a laminar-premixed flame, the luminous region is that portion of the flame where the temperature rise is the greatest and where much of the reaction and heat release occur. The exact ratio of oxidizer to fuel needed for complete combustion is known as the stoichiometric ratio. Flame properties are commonly correlated with the equivalence ratio, which is defined as the stoichiometric oxidizer:fuel ratio divided by the actual oxidizer:fuel ratio. Throughout this work we used a fuel-lean flame with an equivalence ratio of 0.94, which is the optimal condition for oxidizing PP film.[5]

Flame treatment was performed using equipment built by 3M Company. A schematic diagram of the equipment and a description of the flame treatment were published previously.[7] Dust-filtered, $25°C$ compressed air with a dew point of $< -20°C$ was premixed with the natural gas fuel in a venturi mixer located upstream of a 30×1-cm ribbon burner supplied by the Flynn Burner Corporation (New Rochelle, NY). The natural gas had a specific gravity of 0.577, a stoichiometric ratio with air of 9.6:1, and an average heat content of $37.8 \, J/cm^3$. The normalized flame power used in these experiments was $500 \, W/cm^2$ of burner surface area. At this normalized flame power, the tips of the luminous flame cones were ca. 3 mm above the topmost surface of the ribbon burner and about 4 mm from the surface of the PP film.

To generate a range in the extent of PP surface oxidation, we varied the film speed from 100 to 300 m/min while leaving all of the other flame conditions constant. As discussed previously,[8] the total downstream dimension of the zone of reactive product gases is ca. 15 cm so that the exposure time of the film to the active species of the flame varied from 0.03 to 0.09 s.

2.2. Surface Analysis

The PP film samples were analyzed by ESCA, contact-angle measurements, and AFM. ESCA spectra were obtained on a Hewlett-Packard Model 5950A spectrometer using a monochromatic Al Kα photon source at an electron take-off angle with respect to the surface of $38°$. Spectra were referenced with respect to the 285.0 eV carbon 1s level observed for hydrocarbon. No oxygen was detected on the untreated PP. No elements other than oxygen and carbon were detected on any treated PP. Based on repetitive analysis of flame- and corona-treated PP films, we estimate that the standard deviations of the O/C atomic ratios obtained from ESCA are 0.02. This standard deviation indicates the reproducibility of both the treatments and the ESCA technique. ESCA was conducted within several hours of treatment and occasionally thereafter for 180 days.

Measurements of the advancing and receding contact angles in air of deionized, filtered water were made using the Wilhelmy plate method on a Cahn DCA-322 dynamic contact-angle instrument. Using the microbalance, the sur-

face tension of the water was measured as 72.6 mN/m at 20°C. A three-layer laminate was prepared using 3M Scotch Brand #666 double-coated tape to mount the treated sides of the film outward. To prevent contamination during the preparation of this laminate, the treated surfaces only contacted untreated PP film. This situation is analogous to the common practice of winding modified film into roll form after treatment. ESCA, contact-angle, and AFM analysis confirm that no LMWOM is transferred to the untreated side of the PP film during the preparation of the Wilhelmy laminates or during the aging of the treated films. The laminate was cut into a 2.54 × 2.54-cm square for analysis. The stage speed was 50 μm/s with a travel distance of ca. 1 cm. At the position of maximum travel, the motion of the stage was halted for 2 min prior to starting the retraction phase of the Wilhelmy cycle, thereby soaking the sample in water for a period of time. The volume of water used for the contact-angle measurements was ca. 50 cm^3, with a fresh volume of water used for each sample analyzed. The advancing and receding contact angles were calculated using a software routine supplied with the Cahn instrument that uses linear regression for the buoyancy correction. The untreated PP film had advancing and receding water contact angles of 109° and 87°, respectively. Typical standard deviations for the contact-angle measurements were 2°, except for the advancing angles on LMWOM-containing surfaces, which typically had standard deviations of 4°.

Measurements of the water contact angles were made within an hour after treatment of the PP and occasionally thereafter for a period of 180 days. The treated samples were stored in roll form at ambient conditions (18–22°C, 20–50% RH). In addition, the treated films were washed with deionized, filtered water in a controlled fashion using the Cahn instrument. During the measurement of contact angles by the Wilhelmy plate method, washing of the surface is accomplished by the cycle of forcing the PP film into the water bath, holding it for 2 min in the water, and then retracting the film. Approximately 2 min after this washing, we performed a second measurement of the advancing and receding contact angles. This second cycle generated the water contact angles for the water-washed materials. Note that the receding contact angles are always measured on "washed" surfaces because the PP is immersed in water during the measurement of the advancing angle. Hence, no difference in the receding angle for unwashed and washed samples should be expected. This is the behavior that we observe for these flame-treated PP films. Using the Cahn microbalance, we found that the surface tension of the water did not change after these two cycles of immersion. This means that any material that might have dissolved into the water from the PP film did not detectably alter the properties of the water. After the two cycles of washing, the PP samples were analyzed by ESCA or AFM, thereby generating the data for the water-washed materials.

Virtually all surface-treated polymers exhibit contact-angle hysteresis, a measured difference between the advancing and receding contact angles. It is important

to distinguish kinetic hysteresis, which is time or frequency dependent, from thermodynamic hysteresis, which is an invariant property of the surface. In kinetic hysteresis, changes occur to the liquid–solid system on a time scale comparable to the time of measurement so that the observed contact angles appear to change with time. In thermodynamic hysteresis, there are no changes in the observed contact angles during the course of the measurements.

The contact angles that we measured were completely unaffected by up to six additional Wilhelmy immersion cycles performed subsequent to the initial washing of the samples. In addition, the measured contact angles were not affected by the delay time in air between successive cycles (from no delay to 24 h) or by the time of submersion in the water during washing (from seconds to 24 h). The measured water contact angles were also unaffected by the humidity in the environmental chamber of the Cahn DCA during the measurement process, over the range from 5 to 90% RH. Finally, over a range of Wilhelmy stage speeds from 20 to 265 μm/s, all of the contact angles varied by $<3°$ from those reported for the 50 μm/s stage speed. This variation in contact angle as a function of stage speed is extremely small relative to the observed hysteresis on the surface-treated films, which, as will be shown below, can range up to 50° or more. Taken together, these observations are a strong indication that the contact angles measured on the untreated and surface-treated PP are not time dependent, that is, they do not exhibit a kinetic hysteresis.[9] Therefore, the observed contact-angle hysteresis must be thermodynamic.

The untreated and surface-treated PP films were also examined using a Digital Instruments Dimension 5000 SPM atomic force microscope operated in the tapping mode using Olympus Company OMCL-AC160TS etched-silicon cantilever probes, which have nominal spring constants of ca. 42 N/m and resonant frequencies of ca. 270 kHz. The radii of curvature of the probes were estimated to be <10 nm. The typical A_{sp}/A_o setpoint ratio used for imaging was 1.5/2.0, where A_{sp} is the amplitude of the cantilever oscillation (in volts) at the imaging setpoint and A_o is the amplitude of the cantilever oscillation (in volts) in free space. Scan rates were typically 1.2 Hz. For each image, root mean square (rms) roughness values were calculated using Digital Instruments software version 4.42r4. To include those surface structures of primary interest, the rms roughness was calculated for features of less than 250 nm.

To insure that the information that we obtained from AFM accurately represents the topography of our PP films, numerous examinations were made of each pertinent sample. Characteristic images are shown in this paper. Nearly identical images of these same PP surfaces were obtained at 3M with contact-mode AFM using a Nanoscope II microscope and at the University of Western Ontario (M. J. Walzak, Surface Science Western, The University of Western Ontario, London, Ontario, personal communication, 1999) with both non–contact- and contact-mode AFM using a Topometrix Explorer AFM.
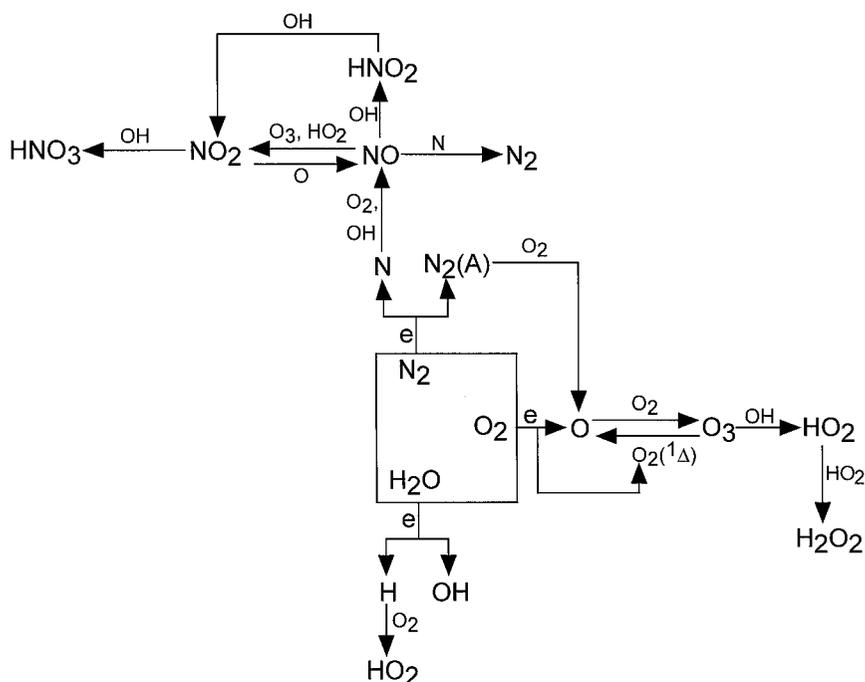
Fig. 1. Gas-phase reaction mechanism for air-corona discharges.

2.3. Gas-Phase Corona Reaction Mechanisms

The simplified reaction mechanism for dry- and humid-air coronas that was used in our computational model is shown in Fig. 1. Rate constants for the heavy particle gas-phase reactions have been obtained from the NIST Chemical Kinetics Database.[10] The electron avalanche that initiates the discharge is caused by ionization of the background gases:
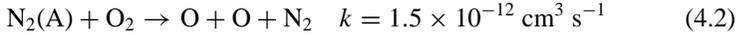
$$e + N_2 \rightarrow N_2^+ + e + e \tag{1.1}$$

$$e + O_2 \rightarrow O_2^+ + e + e \tag{1.2}$$

$$e + H_2O \rightarrow H_2O^+ + e + e \tag{1.3}$$
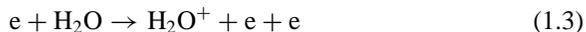
After the discharge pulse, the electrons are lost primarily by dissociative attachment to O_2 and H_2O to form O^- and OH^-, respectively. These ionic species later undergo recombination reactions with positive ions to form neutral species. The chemistry of interest to surface modification usually occurs on longer time scales than these ionic reactions through the various free-radical reactions described below.
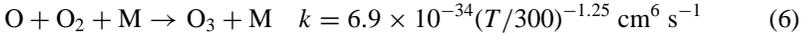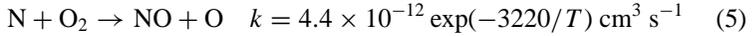
In dry air, the initiating free-radical reactions are the electron-impact disso-ciations of the background gases, N_2 and O_2, that produce N and O atoms:
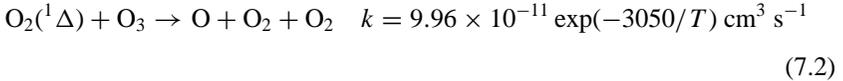
$$e + N_2 \rightarrow N + N + e \qquad (2)$$

$$e + O_2 \rightarrow O + O + e \qquad (3)$$

Oxygen atoms are also produced by the quenching of excited states of N_2, princi-pally $N_2(A)$, by O_2:

$$e + N_2 \rightarrow N_2(A) + e \qquad (4.1)$$

$$N_2(A) + O_2 \rightarrow O + O + N_2 \quad k = 1.5 \times 10^{-12} \text{ cm}^3 \text{ s}^{-1} \qquad (4.2)$$

Subsequent reactions of the O and N radicals include

$$N + O_2 \rightarrow NO + O \quad k = 4.4 \times 10^{-12} \exp(-3220/T) \text{ cm}^3 \text{ s}^{-1} \quad (5)$$

$$O + O_2 + M \rightarrow O_3 + M \quad k = 6.9 \times 10^{-34}(T/300)^{-1.25} \text{ cm}^6 \text{ s}^{-1} \qquad (6)$$
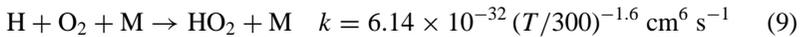
where M is any nonreacting gas-phase species. In a steady-state discharge condi-tion, ozone can be dissociated by reaction with $O_2(^1\Delta)$ to form O and O_2:

$$e + O_2 \rightarrow O_2(^1\Delta) + e \qquad (7.1)$$

$$O_2(^1\Delta) + O_3 \rightarrow O + O_2 + O_2 \quad k = 9.96 \times 10^{-11} \exp(-3050/T) \text{ cm}^3 \text{ s}^{-1}$$
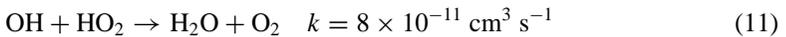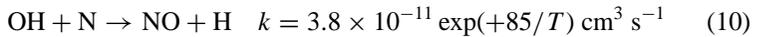
$$(7.2)$$

In practice, no air corona is truly dry; the 2–5% RH discharges used in this study are as low as are encountered in most industrial operations. When water vapor is present in the corona, electron-impact dissociation of H_2O produces H atoms and OH radicals:
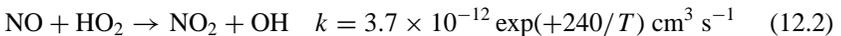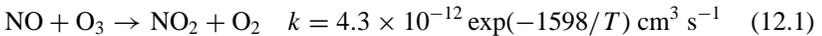
$$e + H_2O \rightarrow H + OH + e \qquad (8)$$

The H atoms react with O_2 to form HO_2 radicals:

$$H + O_2 + M \rightarrow HO_2 + M \quad k = 6.14 \times 10^{-32} (T/300)^{-1.6} \text{ cm}^6 \text{ s}^{-1} \quad (9)$$

The OH radicals can react with N to form NO or with HO_2 to form H_2O and O_2:

$$OH + N \rightarrow NO + H \quad k = 3.8 \times 10^{-11} \exp(+85/T) \text{ cm}^3 \text{ s}^{-1} \quad (10)$$

$$OH + HO_2 \rightarrow H_2O + O_2 \quad k = 8 \times 10^{-11} \text{ cm}^3 \text{ s}^{-1} \qquad (11)$$

Most of the NO formed in the corona is converted to NO_2 by reactions with O_3 and HO_2 radicals:

$$NO + O_3 \rightarrow NO_2 + O_2 \quad k = 4.3 \times 10^{-12} \exp(-1598/T) \text{ cm}^3 \text{ s}^{-1} \quad (12.1)$$

$$NO + HO_2 \rightarrow NO_2 + OH \quad k = 3.7 \times 10^{-12} \exp(+240/T) \text{ cm}^3 \text{ s}^{-1} \quad (12.2)$$

Hydrogen peroxide (H_2O_2) is formed by the reaction of HO_2 with HO_2:

$$HO_2 + HO_2 + M \rightarrow H_2O_2 + O_2 + M \quad k = 1.9 \times 10^{-33} \exp(+980/T) \text{ cm}^6 \text{ s}^{-1}$$

(13)
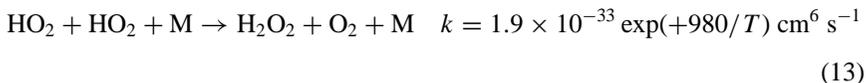
Thus, in industrial coronas in air, in which water vapor is always present to some extent, the active gas-phase species are O, OH, O_2, O_3, HO_2, H_2O_2, N, and NO_x.

The corona-discharge devices that are typically used for the surface modification of polymers are repetitively pulsed by applications of a sinusoidal voltage waveform, usually at frequencies of 5–50 kHz. The electric discharge occurs on the leading edges of the positive and negative voltage waveforms (the "voltage pulse"), producing current pulses of tens of nanoseconds. The charging of the series capacitance in the discharge circuit terminates the current pulse. The plasma formed in the volume of the corona is typically in the form of arrays of microdischarges that are tens to hundreds of micrometers in diameter with area densities of hundreds of microdischarges per square centimeter. Although the charged particles are produced in an inhomogeneous manner, the contribution of ions to the surface treatment is negligible, as discussed below in Section 4. The neutral radicals in the microdischarges have longer lifetimes and larger mobilities than the ions. Thus, to a great degree, diffusion homogenizes the initially nonuniform generation of these species. The end result is that the surface treatment is fairly homogeneous and uniform. There are very few, if any, instances in which industrial corona treatments are considered to be objectionably nonuniform.

2.4. Corona Computational Model

GLOBAL_KIN is a zero-dimensional model used to investigate complex plasma chemistries. It consists of circuit and plasma-chemistry modules.[11] The model has been validated by comparison to experimental data from studies of the plasma remediation of toxic compounds, such as sulfur dioxide and the nitrogen oxides, from effluent streams.[11–13] GLOBAL_KIN models the chemistry in a well-stirred batch reactor based on a user-defined reaction mechanism. The circuit module of the model provides the E/N ratio (electric field/number density) in the plasma, which is then used to obtain the electron–impact reaction-rate coefficients. For this, a table of rate coefficients as a function of electron temperature is generated by solving the Boltzmann equation for electron-energy distribution using a two-term spherical harmonic expansion for several values of the E/N ratio. The equations are integrated as functions of time using VODE, an ordinary-differential-equation solver.[14]

In corona treating, the PP film typically moves at speeds that generate a boundary layer of gas that is drawn through the discharge by the film. The residence time of the gas in the discharge is therefore approximated as being the same as

that of the PP. In this residence time, a given surface area of the polymer and the gas lying above it are exposed to many discharge pulses.

We used computational parameters that best simulated the corona operating conditions described in Section 2.1. The number of voltage pulses that the PP is exposed to is determined by multiplying the voltage frequency by the residence time of the film in the discharge. To model the range of residence times encountered in our experiments, the number of voltage pulses studied was varied from 480 to 67,200. For most simulations of a typical air corona, we used a film speed of 150 m/min for the full downstream electrode length of 12 cm, which corresponds to 921 voltage pulses and a treatment time of ca. 0.05 s. For most of these simulations, we used an inlet gas composition of 79% N_2, 20% O_2, and 1% H_2O, which corresponds to an RH of ca. 28% at 300 K. In a separate series of simulations, the RH in the discharge was varied from 1 to 100%. For an applied voltage of 15 kV, the corona energy was approximately 1.7 J/cm^2.

3. EXPERIMENTAL RESULTS

3.1. LMWOM

Table I shows the surface properties of a number of corona- and flame-treated PP films. The corona and flame treatment conditions were varied to generate a series of PP samples with varying levels of oxidation. All of the treated surfaces have considerable hysteresis ranging from 35 to 60°. The most interesting difference between the two types of treated surfaces is the effect of water washing. In the case of flame-treated PP, washing with water has no effect on the wettability or on

Table I. Surface Properties[a] of Modified Polypropylene Films Before and After Washing With Water

Treatment	ESCA O/C atomic ratio		$\theta_a(°)$[b]		$\theta_r(°)$[b]	
	Unwashed	Washed	Unwashed	Washed	Unwashed	Washed
None	0.0	0.0	110	109	83	83
Flame (0.03 s)	0.07	0.07	97	96	41	42
Flame (0.06 s)	0.12	0.12	94	94	29	29
Flame (0.09 s)	0.18	0.18	84	85	21	21
For RH = 2–5%						
Corona (0.17 J/cm^2)	0.07	0.04	93	97	56	58
Corona (1.7 J/cm^2)	0.12	0.06	76	96	51	53
Corona (17 J/cm^2)	0.23	0.08	59	88	35	36
For RH = 95–100%						
Corona (0.17 J/cm^2)	0.08	0.06	91	97	54	54
Corona (1.7 J/cm^2)	0.12	0.07	75	96	50	51
Corona (17 J/cm^2)	0.23	0.09	54	90	31	30

[a]Properties measured within a few hours of surface treatment.
[b]θ_a and θ_r are the advancing and receding contact angles of water in air, respectively.

the ESCA O/C atomic ratio.[5] As expected,[2–4] however, the surface chemistry of corona-treated PP is strongly affected by water washing, with a significant loss of surface oxidation and a noticeable increase in the advancing contact angle of water. This is clear evidence of the presence of water-soluble LMWOM on the corona-treated PP. Note that flame-treated PP, having an ESCA O/C atomic ratio of 0.18, has no detectable LMWOM, whereas corona-treated polypropylene, having an O/C ratio of only 0.07–0.08, has clearly evident LMWOM.

Using deionized, filtered water, we carefully washed the surface of a large quantity of LMWOM-containing corona-treated PP, collected the solution, passed the liquid through a 1-μm ceramic filter to remove any insoluble contaminants, and then evaporated the water at room temperature in a dry, particulate-filtered air stream. After the water was evaporated, the remaining LMWOM was an oily, highly viscous liquid. We then analyzed this extract by laser-desorption mass spectrometry (LDMS) (L. Hanley, University of Illinois at Chicago, personal communication, 1993–1996). In a typical LDMS experiment, LMWOM was placed onto either clean gold or stainless steel probe tips. Pulsed 1064-nm radiation from a Nb:YAG laser was used to desorb the molecules of LMWOM from the probe tip; the desorbed molecules were then analyzed using an ion-trap mass spectrometer. The LDMS technique enables a quantitative determination of the weight-average molecular weight of the extracted LMWOM. LDMS analysis of the LMWOM from a variety of corona-treated PP films yielded a molecular weight of 400 ± 80 D, with some fragments having molecular weights as low as 100 D. This molecular weight agrees closely with the gel-permeation chromatography results reported by Overney et al.[15] for the water-soluble extract from corona-treated PP.

Analysis of the collected LMWOM using gas chromatography, ^{1}H NMR, IR, and LDMS indicates that the LMWOM arises from cleavage of the PP chain into a series of oligomers containing oxidized groups such as COOH, CHO, or CH_2OH. Evidence of some unsaturation was also observed by NMR. Within the error of the LDMS experiments, the molecular weight of the LMWOM was largely independent of the corona energy or the humidity in the discharge over the range of 2–100%.

Figure 2 shows an AFM image of untreated biaxially oriented PP, showing the characteristic fine fibrillar network that has been observed by numerous researchers.[5,16–21] The diameters of the fibrils are typically <10 nm. The untreated PP has the finest structural features that we have observed with AFM. The fibrillar structure is a result of the quenching and subsequent orientation of the PP.[19]

Figure 3 is a representative AFM image of flame-treated PP having an ESCA O/C atomic ratio of 0.18. Flame treatment alters the fibrils by forming small nodules, which have the appearance of a "bead-like" structure. This structure is much less distinct and of larger characteristic dimensions than the fibrils of the untreated PP. The characteristic size of the nodules is in the submicrometer range.
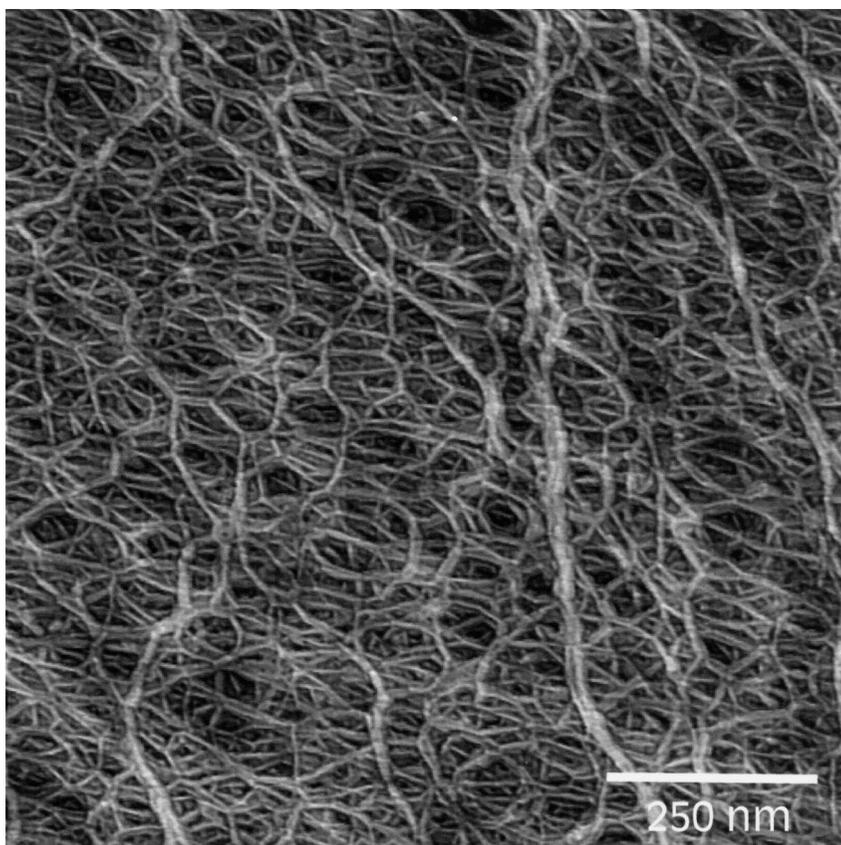
Fig. 2. Tapping-mode AFM topographic image of an untreated biaxially oriented polypropylene film. From the darkest to the lightest tone represents 50 nm of height in the z-direction. The rms roughness of this sample is 0.67 nm.

As discussed in detail in our earlier report on flame-treated PP,[5] the formation of the bead-like structure is not a result of surface heating but is directly associated with the oxidation of the PP by the flame. The nodular topography of the flame-treated materials prepared for this study is not removed or visibly altered by vigorous extraction with water, methanol, acetone, or xylene.[5] The combined contact-angle, ESCA, and AFM results demonstrate that there is no water-soluble material formed on our PP as a result of exposure to the flames used in this study.

By contrast, corona-treated PP shows clear evidence of LMWOM in the AFM images. Figure 4 shows a characteristic image of unwashed PP that was corona-treated at an RH of 95–100% and a corona energy of 1.7 J/cm^2. This material had an O/C atomic ratio of 0.12. The dominant topographical features are smooth,
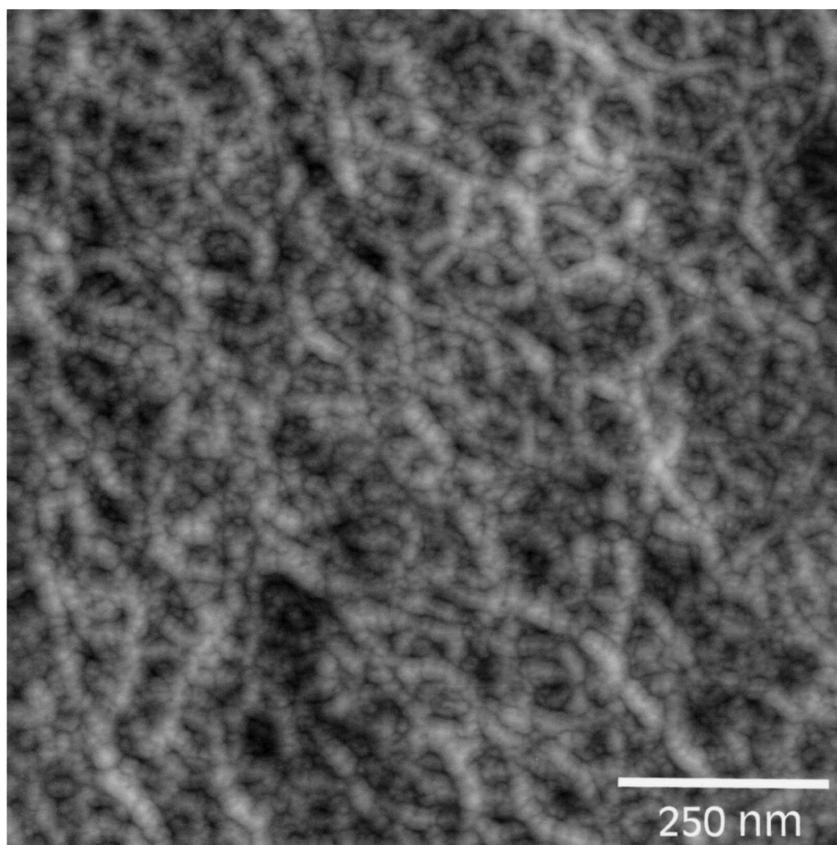
Fig. 3. Tapping-mode AFM topographic image of a flame-treated polypropylene film having an ESCA O/C atomic ratio of 0.18. Washing of the film with water has no detectable effect on surface topography. From the darkest to the lightest tone represents 50 nm of height in the z-direction. The rms roughness of this sample is 0.35 nm.

globular "mounds" that are both much larger and less distinct than either the fibrils of the untreated PP or the nodules formed by flame treatment. The height of the mounds is >50 nm, while the area of a typical mound is ca. 15,000 nm^2. At higher O/C ratios (higher corona energies), still larger mounds are observed (AFM images not shown). Also visible is a smaller secondary structure located amidst the mounds that appears similar to the nodules observed on flame-treated PP.

At lower relative humidities, the mounds are smaller. Figure 5 shows a characteristic AFM image of unwashed PP corona-treated at an RH of 2–5% and a corona energy of 1.7 J/cm^2. This treated material also had an O/C ratio of 0.12. The height of the mounds is ca. 30 nm and the typical area is only ca. 500 nm^2.
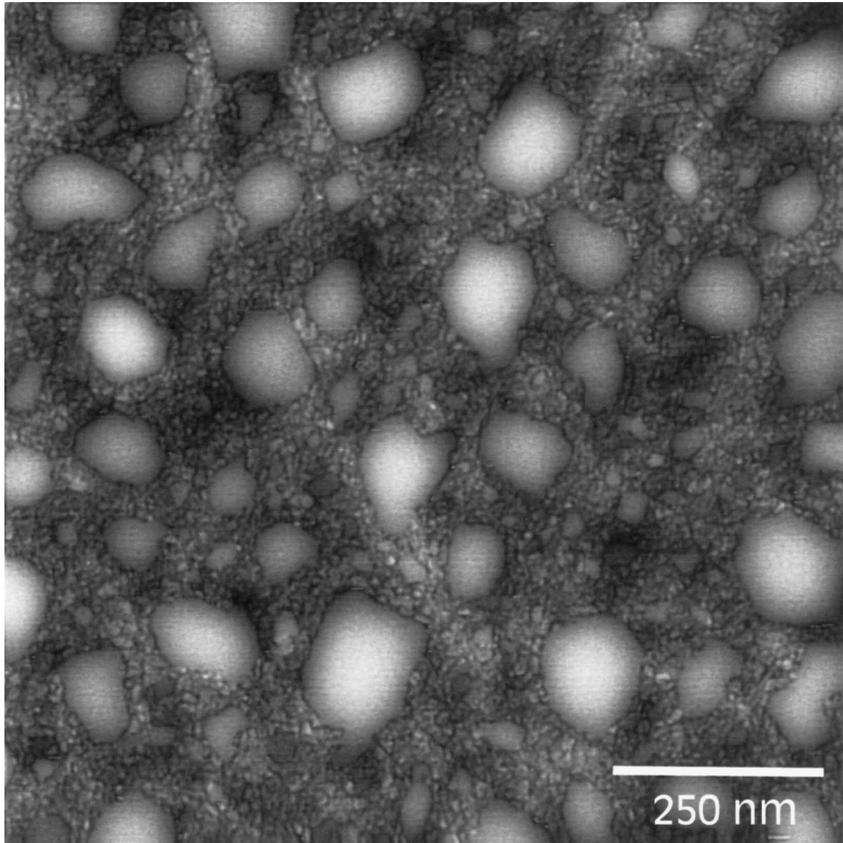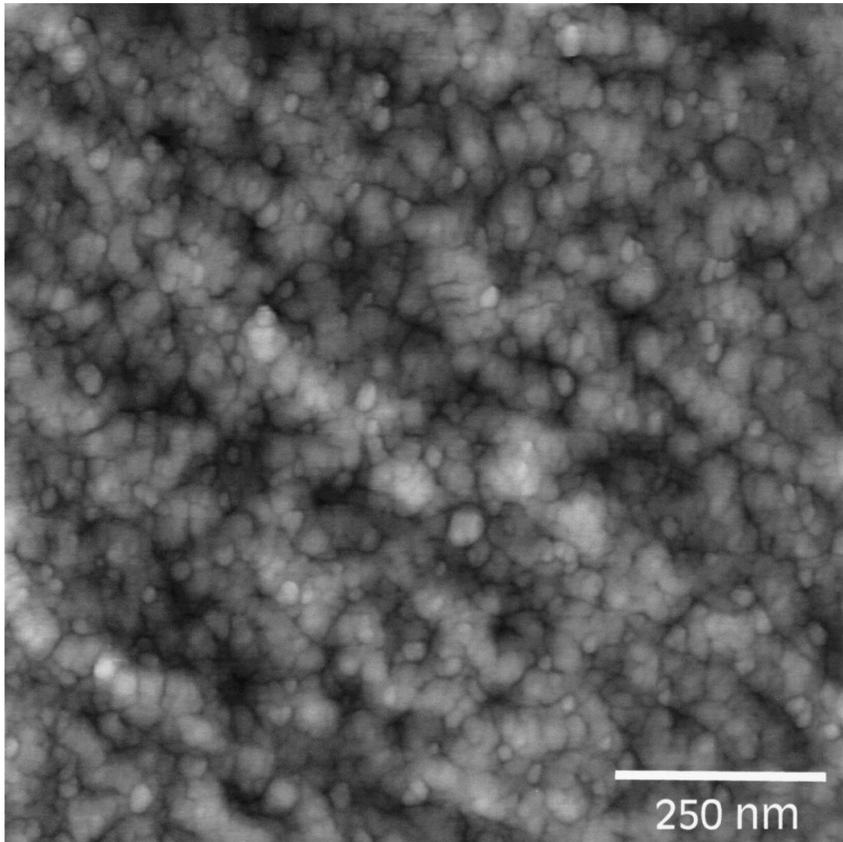
Fig. 4. Tapping-mode AFM topographic image of a polypropylene film treated in an air corona discharge at 95–100% RH and 1.7 J/cm^2. The treated film has an ESCA O/C atomic ratio of 0.12. From the darkest to the lightest tone represents 50 nm of height in the z-direction. The rms roughness of this sample is 0.48 nm.

As shown by Fig. 6, upon washing the PP with water or other polar solvents, the globular mounds are completely removed, revealing a nodular structure that is similar to the topography of flame-treated PP. However, the nodules present on water-washed, corona-treated PP appear more varied in size and are somewhat larger than the nodules formed by flame treatment. The topography of corona-treated films *after* washing with water appears to be independent of the discharge RH. Obviously, the mounds are water-soluble LMWOM that has agglomerated on top of and amidst the nodular structure. The nodular topography of the water-washed corona-treated PP is unaffected by subsequent 24-h extraction with 25°C water or acetone.
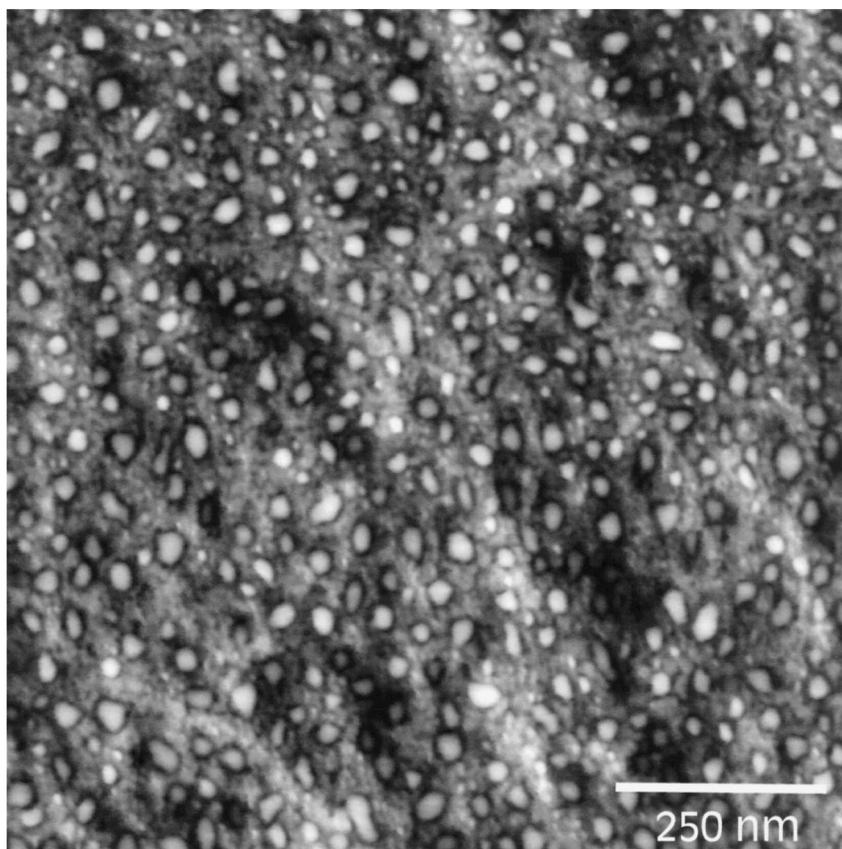
Fig. 5. Tapping-mode AFM topographic image of a polypropylene film treated in an air corona discharge at 2–5% RH and 1.7 J/cm^2. The treated film has an ESCA O/C atomic ratio of 0.12. From the darkest to the lightest tone represents 50 nm of height in the z-direction. The rms roughness of this sample is 0.39 nm.

Our earlier studies of corona-treated PP[2] using scanning electron microscopy (SEM) did not detect any topographical features at low discharge RH, but the mounds of LMWOM detected by AFM at low RH are sufficiently small that we would not have been able to easily observe them using SEM. At a discharge RH of 95–100%, the mounds of LMWOM are much larger than at low RH, thus reaffirming our SEM results from the 1980s.[2] In that earlier work, we used gravimetric methods to prove that more LMWOM was actually formed at low RH than at high RH. It thus appears that large amounts of water vapor *may not* be necessary for the formation of agglomerated mounds of LMWOM, but that the presence of water aids in the aggregation of LMWOM into larger topographical features. In

Fig. 6. Characteristic tapping-mode AFM topographic image of a corona-treated polypropylene film following washing with water. There is no detectable effect of discharge RH on the topography of the treated films following washing. The washed film has an ESCA O/C atomic ratio of 0.06. From the darkest to the lightest tone represents 50 nm of height in the *z*-direction. The rms roughness of this sample of washed PP is 0.36 nm.

summary, the amount of LMWOM formed is greater at low RH, but the size of the agglomerated features increases as the RH in the discharge increases.

For both flame and corona treatments, the fine fibrillar structure of the untreated PP is not restored by any type of washing that we have performed. In addition, we found that annealing of the treated PP for up to 24 h at 100°C in a vacuum oven does not restore the fine topographical features of the untreated PP.

Other researchers have previously observed similar structures on corona-treated PP. In 1993, Overney *et al.*[15] were the first to publish AFM images of corona-treated PP. They observed "droplets" that could be removed by gentle wiping. Overney *et al.* did not generate any images of washed materials. O'Hare

et al.[20], Greenwood et al.,[22] and Boyd et al.[23] observed large, micron-sized globular mounds on corona-treated PP that expanded in size as the corona energy was increased. Both O'Hare et al. and Boyd et al. also reported that, although the mounds disappeared after washing with polar solvents, the fine structure of the untreated PP was not restored. Instead, small topographic features in the 0.1-μm size range remained on the washed surface. Finally, Vancso et al.[24] reported "droplet-like" features on corona-treated PP, which, they stated, confirmed the results of Overney et al. These AFM studies lead to the conclusion that the globular mounds are LMWOM.

All of the recent AFM investigations of corona-treated PP confirm earlier observations made using SEM.[2,25,26] The researchers who used SEM typically found "bumps," "mounds," or a "frosted" surface on PP that was treated in a corona at high energies and/or high humidities. Among the many advantages of AFM is the ability to detect the mounds of LMWOM on PP at the much lower corona energies typically used in industrial treatments. For example, we[2] obtained high quality SEM images of LMWOM mounds only for treatments at corona energies >10 J/cm^2 while O'Hare et al.[20] found that AFM clearly detects the mounds at corona energies as low as 0.5 J/cm^2.

LMWOM generated using other surface-oxidation processes forms topography similar to that produced by corona treatment. Both Greenwood et al.[22] and Mahlberg et al.[27] showed that mounds of LMWOM are formed by the low-pressure oxygen-plasma treatment of PP. Using 3M PP film identical to that used in this work, Nie et al.[18] found that combined UV and ozone (UVO) treatment yields a surface consisting of larger globular mounds and smaller nodules, which correspond to the topographical features that we observe on corona-treated PP. Since Nie et al. found that washing with water removed the larger droplet-like mounds but retained the smaller nodules, they also ascribed the mounds to agglomerated LMWOM.

3.2. Treatment Stability

Table II shows the changes in the properties of representative surface-oxidized PP films after 6 months of ambient aging in roll form. Films treated at conditions

Table II. Changes in the Surface Properties of Modified Polypropylene Films After 6 Months of Ambient Aging

Treatment	Initial O/C atomic ratio	Change in O/C atomic ratio	Change in $\theta_a(°)^a$	Change in $\theta_r(°)^a$
Flame	0.18	0.00	0	+3
Unwashed corona (for RH = 2–5%)	0.12	−0.01	+9	+9
Washed corona	0.06	0.00	+4	+9

$^a\theta_a$ and θ_r are the advancing and receding contact angles of water in air, respectively.

that yield other O/C atomic ratios show similar trends. Long-term aging of flame-treated PP does not cause a significant loss in wettability or in the extent of oxidation. Only the receding contact angle of water decreases over a 180-day period, and then by only $3°$. In contrast, corona-treated PP exhibits more significant changes upon aging. On unwashed corona-treated PP, there are modest increases in both the advancing and receding contact angles that are accompanied by a small decrease in the O/C atomic ratio, which is of the order of the standard deviation in the atomic ratios. For corona-treated PP that is washed with water and then subsequently aged, there is no change in the O/C atomic ratio, but there are still detectable increases in the advancing and receding contact angles.[3] While both treated surfaces are quite stable when compared with, for example, corona-treated poly(ethylene terephthalate) (PET),[4] flame-treated PP is definitely more stable than corona-treated PP.

4. COMPUTATIONAL RESULTS

The electron number densities (n_e) for the first, last, and selected intermediate modeled pulses are shown in Fig. 7(a). The peak n_e is approximately 6×10^{14} cm^{-3}. The electron density during the first pulse is smaller than the densities at later pulses because the dielectric has yet to be charged. During later pulses, the electron density attains a periodic steady state (PSS); the higher densities are the result of the charged dielectric contributing voltage to the gap. Because the concentrations of the major background gases N_2, O_2, and H_2O remain nearly constant over the series of discharge pulses, electron production in the later pulses remains essentially unchanged.

The corresponding electron temperature (T_e) during the pulses is plotted in Fig. 7(b). The peak T_e is approximately 9.5 eV. As in the case of n_e, the difference in T_e between the initial and later pulses occurs because of the incomplete charging of the dielectric. Because of the residual voltage on the dielectric in the later pulses, the E/N ratio is higher, producing a higher T_e and, hence, a more rapid electron avalanche.

The concentrations of O, N, and OH for the first, last, and selected intermediate pulses are shown in Fig. 8(a) and (b). The concentrations of these primary radicals reach an asymptote after hundreds of discharge pulses. Any H atoms formed from water in the discharge are quickly consumed by reactions with O_2 to form HO_2 so that both the lifetime ($\sim\mu$s) and the concentration of H in the discharge are much less than that of O and OH.

The temporal evolution of the densities of the ionic species O_2^+ and N_4^+ is shown in Fig. 8(c). O_2^+ is produced by the electron impact ionization of O_2 (Eq. (1.2)), while N_4^+ is formed by the reaction of N_2 with N_2^+,

$$N_2^+ + N_2 + M \rightarrow N_4^+ + M. \tag{14}$$
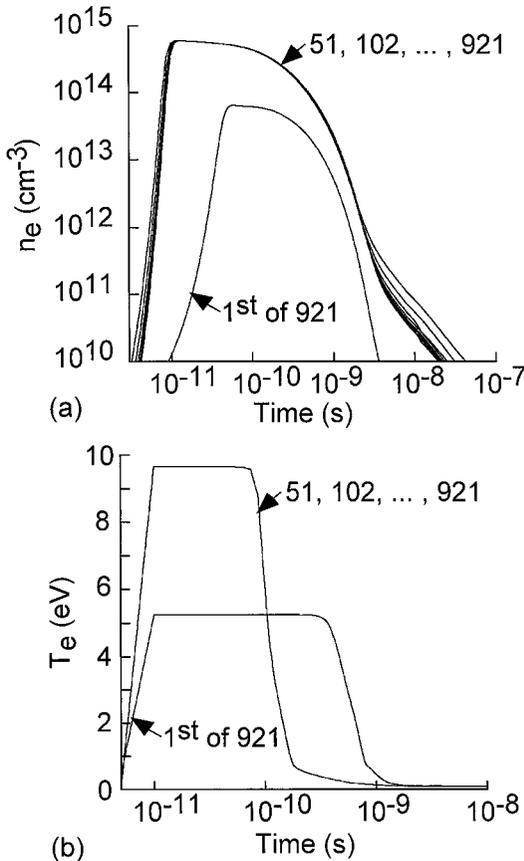
Fig. 7. Discharge properties for the first, the last, and se-
lected intermediate pulses: (a) n_e; (b) T_e. The gas mixture is
$N_2/O_2/H_2O = 79/20/1$ at 300 K and 1 atm pressure. Electron
densities during the first pulse differ from those of the later
pulses because of the smaller voltage across the gap resulting
from the incomplete charging of the dielectric. Correspond-
ingly, T_e is also smaller during the first pulse. After 10 s of
pulses, the electron density and temperature reach a periodic
steady-state (PSS). The electron density and temperature re-
main the same during the later pulses because the density of
the background gases does not change significantly. The ap-
plied voltage is 15 kV and the corona energy is 1.7 J/cm^2.

In general, the ions are consumed faster than the radicals are. As a result, the time-
averaged concentrations of ions are much smaller than that of the radicals. Hence,
the ion chemistry at the surface can be safely neglected. An additional reason for
neglecting ion chemistry in corona treatment is that the ions arriving at the PP
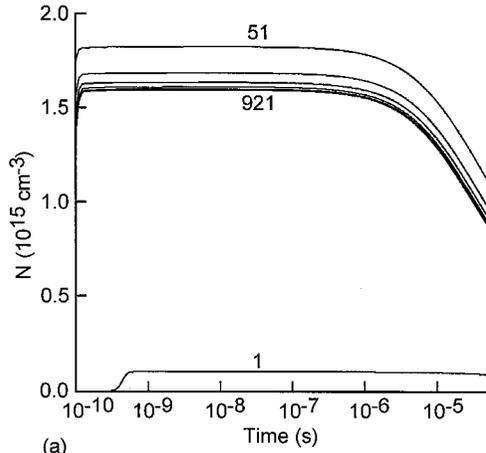
(a)
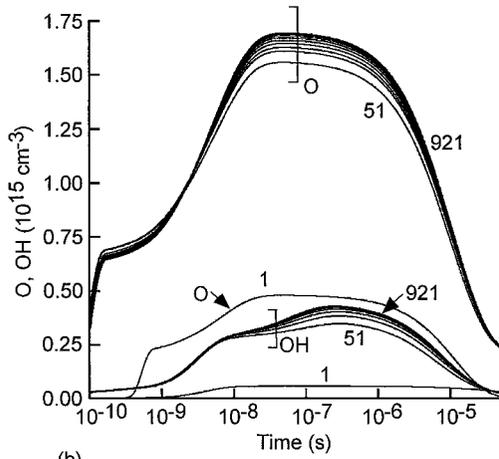
(b)
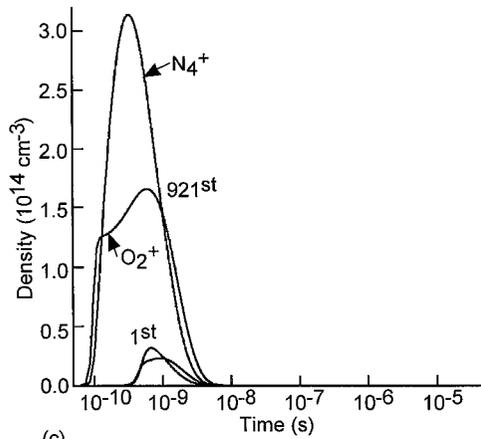
(c)

surface are thermal. This is a result of two facts. Firstly, for most of the time that the polymer is in the discharge, the voltage across the electrode gap is nearly zero. Hence, there is no external electrical field to accelerate the ions toward the surface. Secondly, many collisions occur in the sheath region of an atmospheric-pressure discharge so that those ions that *do* arrive at the surface are thermal.

4.1. Effect of Corona Energy

As discussed above, as the corona energy increases, the extent of oxidation and the amount of LMWOM produced also increases. To examine the effect of corona energy on the gas-phase species, the time-averaged number concentrations of O and OH were calculated for selected energies.

The PSS electron densities are shown in Fig. 9(a) for normalized energies of 0.9, 1.3, 1.7, 2.0, and 2.4 J/cm^2, which correspond to applied voltages of 10.0, 12.5, 15.0, 17.5, and 20.0 kV, respectively. The RH for these cases is ca. 28%. At the higher applied voltages, the electron-impact rate coefficients are larger thereby initiating a more rapid avalanche. The PSS densities of O atoms and OH radicals resulting from this avalanche are shown in Fig. 9(b) and (c). With increasing corona energy, the increased electron density produces more dissociation of O_2 and H_2O, resulting in the increased production of O and OH. The primary loss process for O atoms is by reaction with O_2 to form O_3 (Eq. (6)). OH radicals are mainly consumed by reactions with N and HO_2 (Eq. (10) and (11)) to form NO and H_2O. For our conditions, NO concentrations are a few ppm while NO_2 concentrations are a few tenths of a ppm.

The time-averaged concentrations of selected species were calculated according to the equation:

$$< N_i > = \frac{\int_0^\tau N_i dt}{\tau}$$

where $< N_i >$ is the time-averaged concentration, N_i is the instantaneous concentration of species i, and τ is the residence time of the PP in the discharge. These time-averaged values provide a sense of the species concentration that affects the PP surface during passage through the discharge.

The ratio of the time-averaged concentrations of O, denoted by <O>, to OH, denoted by <OH>, as a function of corona energy is shown in Fig. 10(a). As the

Fig. 8. Densities of primary radicals and ions for the first, the last, and selected intermediate pulses: (a) N; (b) O and OH; (c) $O_2{}^+$ and $N_4{}^+$. Conditions are the same as described for Fig. 7. The difference in the densities of the ions and radicals between the first and later pulses is due to the difference in the production of electrons arising from the incomplete charging of the dielectric. After 100s of discharge pulses, the radicals attain a PSS. Ions attain a periodic steady-state (PSS) in densities more quickly, in a few discharge pulses. Ions are consumed much faster as compared with the radicals.
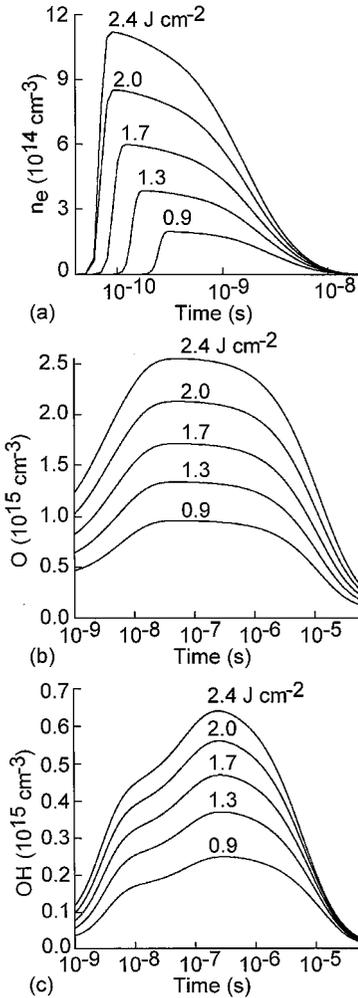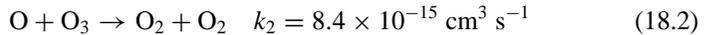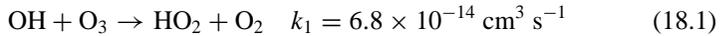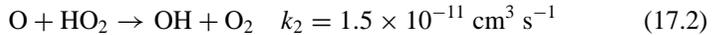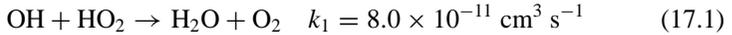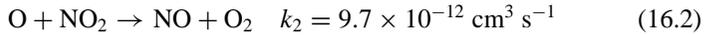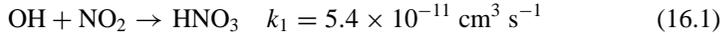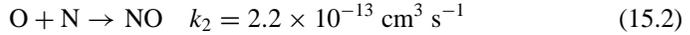
Fig. 9. Periodic steady-state (PSS) densities of electrons and radicals as a function of energy deposition: (a) n_e; (b) O; (c) OH. Conditions are the same as described for Fig. 7. Corona energies of 0.9, 1.3, 1.7, 2.0, and 2.4 J/cm^2 correspond to applied voltages of 10.0, 12.5, 15.0, 17.5, and 20.0 kV, respectively. Higher applied voltages produce hotter electrons resulting in higher electron densities and a more rapid avalanche. This results in increased rates of dissociation of the background gases, thereby producing more O and OH. For a given energy deposition, peak OH concentrations are smaller than peak O-atom concentrations.

corona energy increases, the <O>/<OH> ratio also increases. The proportion of the corona energy channeled into the reactions that lead to the direct and indirect production of O and OH as a function of the E/N ratio is shown in Fig. 10(b). For applied voltages of 10–20 kV, the E/N ratio is 270–540 Td (1 Td = 1 × 10^{-17} V cm^2). In this range, most of the energy deposition is channeled into the excitation of N$_2$ and O$_2$. Through the reactions with O$_2$ and O$_3$ (Eqs. (4.2) and (7.2)), the increased densities of N$_2$(A) and O$_2$($^1\Delta$) produce more O. Although the fractional energy expended for the dissociation of H$_2$O to produce OH also increases with increasing E/N ratio, the absolute increase is small.
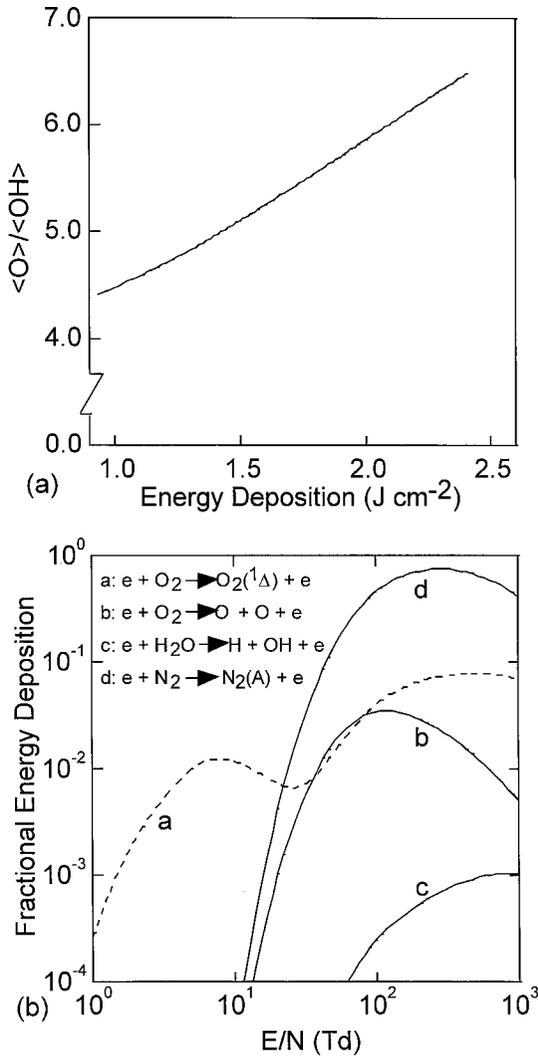
Fig. 10. Effect of corona energy on the time-averaged concentrations of O and OH: (a) $<O>/<OH>$ as a function of corona energy; (b) fractional energy deposition into the electron-impact reactions resulting in the direct and indirect production of O and OH. At the E/N ratios of interest (100s of Td; 1 Td $= 1 \times 10^{-17}$ V cm^2), most of the input energy goes into the vibrational excitation of N_2 (producing $N_2(A)$) and the electronic excitation of O_2 (producing $O_2(^1\Delta)$). Both $N_2(A)$ and $O_2(^1\Delta)$ produce O by reaction with O_2 and O_3 (Eqs. (4.2) and (7.2)). Hence, as the E/N ratio increases, O-atom production increases. Conditions are the same as in Fig. 7.

The increase in $<O>/<OH>$ with energy is also caused, in part, by the higher gas-phase reactivity of OH relative to O, which results in a higher consumption of OH in the corona. For example, the rate coefficients at 298 K for the reactions of O and OH with various reactants are:

$$OH + N \rightarrow NO + H \quad k_1 = 5.0 \times 10^{-11} \text{ cm}^3 \text{ s}^{-1} \tag{15.1}$$

$$O + N \rightarrow NO \quad k_2 = 2.2 \times 10^{-13} \text{ cm}^3 \text{ s}^{-1} \tag{15.2}$$

$$OH + NO_2 \rightarrow HNO_3 \quad k_1 = 5.4 \times 10^{-11} \text{ cm}^3 \text{ s}^{-1} \tag{16.1}$$

$$O + NO_2 \rightarrow NO + O_2 \quad k_2 = 9.7 \times 10^{-12} \text{ cm}^3 \text{ s}^{-1} \tag{16.2}$$

$$OH + HO_2 \rightarrow H_2O + O_2 \quad k_1 = 8.0 \times 10^{-11} \text{ cm}^3 \text{ s}^{-1} \tag{17.1}$$

$$O + HO_2 \rightarrow OH + O_2 \quad k_2 = 1.5 \times 10^{-11} \text{ cm}^3 \text{ s}^{-1} \tag{17.2}$$

$$OH + O_3 \rightarrow HO_2 + O_2 \quad k_1 = 6.8 \times 10^{-14} \text{ cm}^3 \text{ s}^{-1} \tag{18.1}$$

$$O + O_3 \rightarrow O_2 + O_2 \quad k_2 = 8.4 \times 10^{-15} \text{ cm}^3 \text{ s}^{-1} \tag{18.2}$$

In all cases, OH is more reactive than O. Thus, not only is a smaller amount of OH produced as compared with O, but the OH that is produced is then consumed more rapidly than the O. The net result is a lower time-averaged concentration of OH as compared with O.

Some of the O-atom consuming reactions are reversible. For example, the consumption of O by O_2 to form O_3 (Eq. (6)) is followed by O_3 conversion back to O by the reaction with $O_2(^1\Delta)$ (Eq. (7.2)). With this cyclic process, higher O atom concentrations can be maintained, which also leads to higher $<O>/<OH>$ ratios.

One of the notable gaseous products of air-corona processing is O_3. The time-averaged concentration of O_3 as a function of corona energy is shown in Fig. 11. The primary loss processes for O_3 are the reactions with $O_2(^1\Delta)$ (Eq. (7.2)) and H:

$$H + O_3 \rightarrow OH + O_2 \quad k = 1.4 \times 10^{-10} \exp(-470/T) \text{ cm}^3 \text{ s}^{-1} \tag{19}$$
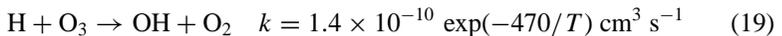
The modeling results shown in Fig. 11 agree with the observation[28] that ozone production in a corona treater increases relatively linearly with corona power at low power loadings.

Another product of an air corona is H_2O_2. The time-averaged concentrations of H_2O_2 and HO_2 as a function of corona energy are also shown in Fig. 11. With increasing energy, more H is produced by the electron impact dissociation of H_2O (Eq. (8)), which then reacts with O_2 to form HO_2 (Eq. (9)). HO_2 then reacts with itself to produce H_2O_2 (Eq. (13)).

4.2. Effect of Relative Humidity

The ratio of the time-averaged concentrations of O and OH as a function of RH is shown in Fig. 12 for a corona energy of 1.7 J/cm^2. With increasing RH,
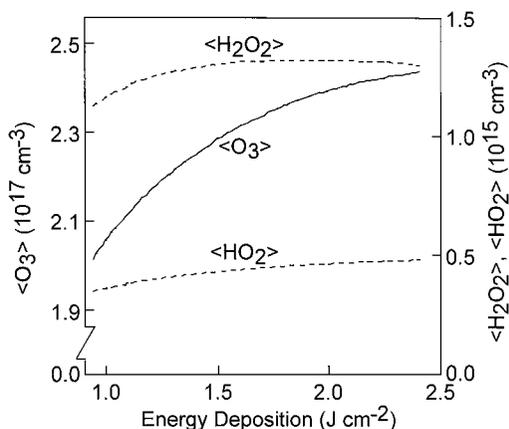
Fig. 11. Time-averaged concentrations of O_3, H_2O_2, and HO_2 as a function of corona energy. O_3 is produced by the reaction of O atoms with O_2 (Eq. (6)). H_2O_2 is produced by the reaction of HO_2 with itself (Eq. (13)). With increasing energy deposition, larger amounts of O and H atoms are produced by the electron-impact dissociation of O_2 and H_2O, which then produce more O_3 and HO_2 (Eqs. (6) and (9)). Increased HO_2 formation leads to the increased production of H_2O_2. Conditions are the same as in Fig. 7.

<O>/<OH> decreases due to the increase in <OH> that results from the higher rates of electron-impact dissociation of H_2O. As a disproportionate amount of power is dissipated into the H_2O, less power is available for O-atom production. Hence <O> decreases and as a result, <O_3> also decreases as RH is increased (Fig. 12). This result again agrees with the observation that ozone production in coronas and ozonizers decreases as RH increases.[28] The qualitative agreement between experimentally determined ozone production rates, both as a function of energy and of RH, and our modeling data for ozone production provides a meaningful validation of the computational model used in this study.

4.3. Comparison of Corona Gas-Phase Chemistry to Flame Gas-Phase Chemistry

In 2001, we reported[5] on the use of SPIN to model the chemistry of impinging air–hydrocarbon flames. The SPIN modeling results allowed us to relate the flame equivalence ratio to the flame chemistry, which was then correlated to the surface oxidation generated by the flame treatment. For PP, optimal oxidation occurs at an equivalence ratio of ca. 0.94, which is the equivalence ratio used to prepare all of the flame-treated PP films used in this study. As calculated by SPIN, the mole fractions of the important gas-phase species at the surface of the PP at an equivalence ratio of 0.94 are listed in Table III. In addition, in a fuel-lean flame, there is considerable
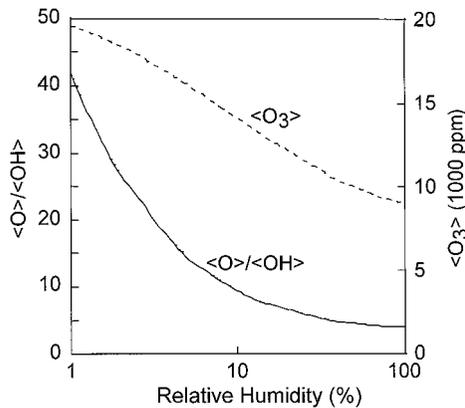
Fig. 12. Variation of $<O>/<OH>$ and $<O_3>$ as a function of RH at a corona energy of 1.7 J/cm^2. At higher RH, more energy is channeled into OH production resulting in a decreased $<O>/<OH>$. $<O>$ decreases with increasing RH because of the decreased rate of dissociation of O_2. As a result, $<O_3>$ decreases.

free O_2 present from the excess air, but no ozone. Thus, the optimal flame conditions for oxidizing PP are characterized by high concentrations of the oxidizing species OH, HO_2, H_2O_2, and O_2 coupled with relatively low concentrations of H and O atoms.[5] The ratio of [O]:[OH] in this type of flame is ca. 0.006.

Table III also lists the time-averaged concentrations of the same gas-phase species in the corona at low and high RH. An air corona is characterized by high concentrations of O, HO_2, H_2O_2, and O_3, but a relatively low concentration of OH and virtually no H atoms. In a corona, the $<O>:<OH>$ ratio decreases from ca.

Table III. Concentrations and Ratios of Some of the Important Gas-Phase Reactive Species in a Flame and an Air Corona

Species	Mole fractions in a fuel-lean flame[a]	Time-averaged concentrations[b] in an air corona	
		at RH = 1%	at RH = 100%
OH	51.4×10^{-6}	0.18×10^{14}	1.34×10^{14}
HO_2	30.4×10^{-6}	1.46×10^{14}	5.00×10^{14}
H_2O_2	18.7×10^{-6}	4.98×10^{14}	16.0×10^{14}
H	15.9×10^{-6}	0.002×10^{14}	0.016×10^{14}
O	0.3×10^{-6}	7.57×10^{14}	4.88×10^{14}
O_3	$<10^{-12}$	4700×10^{14}	1800×10^{14}
O/OH	0.006	42.1	3.63

[a] At an equivalence ratio of 0.94.
[b] Concentrations in species per cm^3.

42 to 4 as the RH increases from 1 to 100%.

## 5. DISCUSSION

5.1. Oxidation and Chain Scission

On PP, LMWOM is much less likely to form during flame treatment than during corona treatment. With coronas, LMWOM is easily detected at an O/C atomic ratio as low as 0.06, while with flame treatment, no LMWOM is observed at an O/C = 0.18. A high level of oxidation alone is clearly not sufficient to form water-soluble LMWOM. Corona treatment must also cause a much greater reduction in the molecular weight of the PP during oxidation than does flame treatment.

For polypropylene, it is widely accepted[29–32] that chain scission and the lowering of the molecular weight of oxidized PP occur primarily through the β-scission reaction:
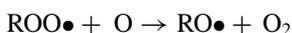
$$-C-C(O\bullet)-C \rightarrow -C=O + \bullet C-$$
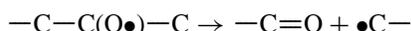
Polymer alkoxy radicals are, therefore, the principal precursor to LMWOM. There are several routes to alkoxy-radical formation in PP oxidation mechanisms:
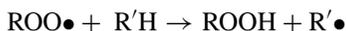
1. the direct formation of alkoxy radicals from the reaction of polymer alkyl radicals with atomic oxygen:

$$R\bullet + O \rightarrow RO\bullet$$
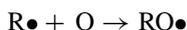
2. the reaction of polymer peroxy groups with atomic O:

$$ROO\bullet + O \rightarrow RO\bullet + O_2$$

3. the reaction of peroxy groups to form hydroperoxy groups, which subsequently decompose to form alkoxy groups:

$$ROO\bullet + R'H \rightarrow ROOH + R'\bullet$$

$$ROOH \rightarrow RO\bullet + OH$$

4. and the reaction of ozone with alkyl radicals:[33]

$$R\bullet + O_3 \rightarrow RO\bullet + O_2$$
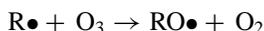
Polymer peroxy or hydroperoxy groups can be formed by the reactions of O_2, HO_2, or H_2O_2 with alkyl radicals:

$$R\bullet + O_2 \rightarrow ROO\bullet$$

$$R\bullet + HO_2 \rightarrow ROOH$$

$$R\bullet + H_2O_2 \rightarrow ROO\bullet + H_2 \ \text{or} \ ROH + OH$$
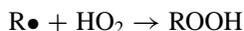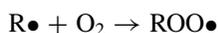
However, Hansen *et al.*[34] state that, when atomic oxygen is present, the peroxy/hydroperoxy route to chain scission is unimportant relative to the reactions involving atomic oxygen. The hydroperoxy route to scission is simply too slow to account for the formation of LMWOM in the short exposure times that are typically encountered in industrial surface-oxidation processes.[5] Therefore, extensive chain scission and the formation of LMWOM should be associated with reactions involving atomic oxygen. As we discuss below, a major difference between the gas-phase chemistry of corona discharges and that of flames is the relative amounts of ozone, O atoms, and OH radicals. In a corona, ozone and O atoms are predominant, while in a flame, the OH radical is the dominant oxygen-containing species in the gas phase.

The influence of UV or vacuum UV radiation on polymer surface modification by plasmas has been investigated by a number of researchers,[35,36] who have concluded that the oxidation of polymer surfaces by O atoms is greatly enhanced when the surface is concurrently illuminated by UV photons. Although UV illumination may play an important role in low pressure plasmas, the contribution of UV radiation in corona treatment is likely to be small. The UV radiation is produced only during the discharge pulse from excited states that have short lifetimes. The duty cycle of illumination is therefore small so that the opportunities for synergistic effects are also small as compared to continuously operated low-pressure plasmas. Even with higher duty cycles, the contributions of UV radiation to surface modification in corona discharges sustained at atmospheric pressure are likely to be small because of the short mean-free-path for absorption of the radiation by gas-phase species.

As noted above, computational modeling of flame treatment[5] showed that the concentration of atomic oxygen at the PP surface was relatively low. The ratio of O to OH at the PP surface was ca. 0.006. We then hypothesized that the lack of detectable LMWOM on flame-treated PP was a result of this low concentration of atomic oxygen in the flame. In flames, oxidation of the PP occurs through the reactions of H, OH, HO_2, H_2O_2, and O_2, without the LMWOM formation that is associated with extensive O-atom reactions. This explained the lack of LMWOM formation, but did not explain the formation of the nodules observed by AFM. During flame treatment, we believe that scission of the PP occurs only to a limited extent through alkoxy radicals formed by the small numbers of O atoms present in the flame coupled with the slower hydroperoxy route to scission described above. This limited scission of the PP lowers the molecular weight of the surface region, but does not quickly generate oxidized chains of sufficiently low molecular weight to be water soluble. These non–water-soluble, intermediate-molecular-weight products may be tethered to the unmodified PP chains by only a few bonds, thereby enabling increased mobility relative to the bulk unoxidized PP. This increased mobility enables the oxidation products to agglomerate to a certain extent in a fashion analogous to the formation of the globular mounds of

LMWOM observed by AFM on corona-treated PP. The net result of limited chain scission and this modest agglomeration is the formation of the nodules observed on flame-treated PP.

An alternate hypothesis for the lack of observable LMWOM on flame-treated PP is that LMWOM is formed by flame oxidation, but is then quickly lost by migration or evaporation. To determine the likelihood of this happening in the flame, we exposed LMWOM-containing corona-treated PP (O/C = 0.12) to 150–160°C for 10 s in a convection oven. AFM and ESCA examinations before and after this heat treatment showed no change to the surface. This strongly implies that, even when present in large quantities, LMWOM does not evaporate or migrate away from the surface in less than a few seconds, even when heated to near the bulk melting point of the PP. So, if the flame were to form any LMWOM, it should not disappear from the surface in the <0.1 s that the film is exposed to the high temperatures of the flame. We therefore conclude that LMWOM is simply not formed to any great extent in flame treatments.

In contrast to a flame, O atoms are a dominant species in the gas phase of a corona; OH radicals are much less common in coronas relative to flames. As shown in Fig. 12 and Table III, in industrial coronas, O concentrations are significantly higher than OH concentrations. Our computational results compare favorably with other studies. Rosocha and Korzekwa[37] report that the ratio of the concentration of $O(^3P)$ atoms to the concentration of OH radicals in a "humid" corona discharge is about 10:1. Gentile and Kushner[11] modeled a dielectric-barrier (corona) discharge at "high RH," finding that the ratio of <O>:<OH> was about 8:1.

There is a significant concentration of N atoms in a corona discharge, yet no nitrogen is detected by ESCA on the treated PP surface, even at the high O/C ratios of 0.23. In their recent careful ESCA study, O'Hare et al.[20] also found only oxidation occurring during the corona treatment of PP. Analysis of corona-treated PP by static secondary ion mass spectrometry (SSIMS) detects trace amounts of oxidized nitrogen species on the surface at negative ion masses of 46 and 62 D. No other nitrogen-containing ion clusters are detected. These trace amounts of oxidized nitrogen can be readily assigned to the reactions of the small quantities of NO and NO_2 in the corona with the PP.[8] Despite a relatively high gas-phase concentration, N atoms do not appear to add to PP surfaces. The reaction mechanism appears to be exclusively dominated by the oxygen-containing species in the corona.

A possible explanation for this lack of affixed nitrogen is that atomic nitrogen reacts with organic molecules primarily by abstraction or scission, rather than by insertion.[38,39] Thus, reactions such as

$$R + N \rightarrow R\bullet + HCN$$

$$R\bullet + N \rightarrow R'\bullet + HCN$$
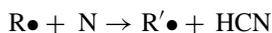
may be most likely reactions of the N formed in a corona with PP. These types of reactions form nitrogen-containing gas-phase products rather than affix nitrogen to polymer surfaces.

Both Kill *et al.*[40] and Moss *et al.*[31] showed that the concentration of O atoms is high in air or oxygen glow discharges. These plasma treatments also form detectable, water-soluble LMWOM, as documented by a number of researchers.[21,25,41–43] In UVO treating, oxygen atoms and molecules are the only significant gas-phase reactive species.[44,45] As noted above, UVO treatment of PP yields LMWOM and surface topographical structures nearly identical to corona treatment. These observations strongly support the contention that O atoms are primarily responsible for LMWOM formation.

Additionally, our previous study[44] showed that the oxidation of PP with ozone only does not lead to the formation of detectable amounts of LMWOM. In ozone treatments, there is little, if any, atomic oxygen. The key reaction in ozone treatments is

$$RH + O_3 \rightarrow ROO\bullet + OH$$
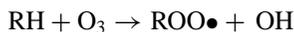
This reaction starts the hydroperoxy route to chain scission, which is too slow to generate detectable LMWOM in surface-modification reactions. Our work on ozone treatments also supports the contention that O-atom reactions are needed for LMWOM formation.

Thus, in air-corona, UVO, and oxidizing-plasma treatments, atomic oxygen leads to rapid chain scission. Widespread chain scission quickly leads to the formation of water-soluble LMWOM. Obviously, if LMWOM is formed from PP, there should also be scission products with intermediate molecular weights. As noted above, these non-water-soluble scission fragments will be more mobile than the bulk polymer. This increased mobility should enable the intermediate-weight oxidation products to agglomerate to some extent, thereby forming the nodules that are observed in conjunction with the globular LMWOM mounds on corona- and UVO-treated PP. Thus, for all types of surface-oxidation processes on PP, it seems likely that nodular topography is generated by the agglomeration and ordering of non–water-soluble intermediate-molecular-weight scission products.

Because nodules form in low-temperature corona, UVO, and plasma treatments, heating of the surface is not required for the formation of the nodules. This supports our earlier contention[5] that the topographical changes observed on flame-treated PP are the result of oxidation rather than of heating. The effects of relative humidity on the topography of corona-treated PP imply that water vapor adsorbed on the PP surface may enhance the mobility of both LMWOM and any intermediate-molecular-weight scission products. In flame treatment, the moist, elevated-temperature environment of the flame should enhance the mobility of the oxidized scission products, even though they are not soluble in water.

During the corona treatment of PP, increasing the RH in the discharge seems to enhance the agglomeration of LMWOM into mounds, but actually decreases the total amount of LMWOM formed. This behavior is readily explained by the fact that the ratio of O to OH decreases as the amount of water vapor in the discharge increases. As the concentration of O atoms declines, less scission occurs, so that there is less formation of LMWOM. However, the LMWOM that is formed is more likely to agglomerate because of the added mobility imparted by adsorbed water.

As we explained previously,[5] the nodules are not likely to be PP crystalline lamella revealed by the oxidative "etching" of amorphous PP material. Any crystalline structure exposed by the removal of amorphous material should be smaller than the fibrils observed on the untreated film. Instead, we observe a gradual increase in the characteristic size of the features formed by surface oxidation. This contention is strongly supported by the earlier work of Mahlberg *et al.*,[27] who state that etching cannot be the explanation for the topographical changes observed on oxygen-plasma-treated unoriented PP because the size of the surface features increases with increasing extent of oxidation.

5.2. Treatment Stability

Decreases in the extent of oxidation or losses in wettability as a function of aging are usually attributed to the reorientation or localized migration of oxidized functional groups located near the surface of a modified PP. As the molecular weight of the surface region decreases, the tendency for functional-group reorientation or migration should increase. The molecular weight of a corona-treated PP surface is lower than that of a flame-treated PP surface. Therefore, corona-treated PP is less stable than flame-treated PP. The AFM images of washed corona-treated PP (Fig. 6) suggest that the molecular weight of the washed surface may be lower than that of the washed flame-treated PP (Fig. 2). Treatment stability is an example of how the surface molecular weight can be more important than the extent of oxidation in determining a practical performance property.

5.3. Contact-Angle Measurements

Surface roughness or surface chemical heterogeneity[9,46,47] causes *thermodynamic* contact-angle hysteresis, such as that observed on the surface-oxidized PP produced for this study. On chemically heterogeneous surfaces, the advancing contact angle is more sensitive to the low energy, unmodified components of the surface, while the receding angle is more sensitive to the high energy, oxidized groups introduced by treatment. Therefore, the receding contact angle is actually the measurement most characteristic of the modified component of a surface. To best characterize any surface-oxidized polymer, both the advancing and receding contact angles should be examined, with the receding angle actually being the more important measurement.

Our untreated PP exhibits considerable contact-angle hysteresis ($22°$). We believe that this hysteresis is not caused by chemical heterogeneity because the film is produced from a homopolymer PP resin and careful ESCA or SSIMS do not detect any additives at the film surface. Thus, the hysteresis must either be caused by surface roughness or by domains of different polymer morphology (crystallinity) on the PP surface or by some combination of the two. Past consensus has been that surface heterogeneity needs to be of the order of 0.1–0.5 μm for roughness and 0.1 μm for chemistry[9,46,47] to affect contact-angle measurements. Some researchers, however, report a limit as low as 0.05 μm[47] for roughness-induced hysteresis. More recently, Youngblood and McCarthy[48] showed that roughness on the nanometer scale can contribute to contact-angle hysteresis. Our untreated PP has considerable structure on the submicrometer scale, with individual fibrils having dimensions of 10 nm or less. It is therefore probable that this topography is the major contributor to contact-angle hysteresis on untreated PP films.

At low levels of flame-generated oxidation (O/C < ca. 0.07), there is no AFM-detectable change in surface topography.[5] Nevertheless, there is a marked increase in the extent of contact-angle hysteresis, from $22°$ for the untreated PP to ca. $55°$ for flame-treated PP with an O/C = 0.07. Relative to the untreated PP, the changes in the advancing and receding contact angles and the further increase in the hysteresis must therefore be caused by heterogeneous oxidation rather than by topographical changes. In semicrystalline polymers such as PP, it is widely believed[49–52] that oxidation occurs mainly in the amorphous and interphase regions. The amorphous regions of the PP are more accessible to the diffusion of the gas-phase reactive species. Gaseous species will not be able to quickly diffuse into the PP lamellae, so that those portions of the PP will be more resistant to oxidation. This heterogeneity in the physical structure of semicrystalline polymers leads to heterogeneity in the surface chemistry of those polymers. In addition, further studies[49,53] suggest that inhomogeneity in the extent of oxidation may be an inherent property of PP molecules. An inhomogeneous distribution of oxidized functional groups can lead to a mixture of highly oxidized small molecules together with relatively intact macromolecules. This type of surface structure would cause the increased contact-angle hysteresis observed for flame-treated PP at low levels of oxidation.

For all of the corona-treated PP that we studied, as well as for the more highly oxidized flame-treated PP (O/C > ca. 0.10), surface topographical changes accompany oxidation. On some of these surfaces, the contact-angle hysteresis can approach $65°$. For these films, the increase in the amount of hysteresis could be caused by both chemical heterogeneity and by the topographical changes to the surface. In the extreme case of LMWOM formation, the advancing angles on unwashed surfaces are affected by the dissolution of the LMWOM into the water, as evidenced by the major increase in the advancing angle on the washed materials and the greater scatter (higher standard deviation) in the data.

While microscopic chemical heterogeneity seems to be the most likely cause for the contact-angle hysteresis on surface-oxidized polymers, there is an alternative explanation. Yasuda *et al.*[54,55] suggest that contact-angle hysteresis can be associated with the rapid reorientation of hydrophilic functionalities. During the measurement of the advancing contact angle, the water front encounters a polymer–air interface where the concentration of hydrophilic groups is low; hence the measured advancing angle is large. During the measurement of the receding angle, the water front traverses a polymer-water interface where the concentration of hydrophilic groups is high; hence the measured receding angle is low. Chan[47] believes that this type of behavior can only occur on the surface of a polymer with extremely high chain mobility, such as a hydrogel material. However, it is conceivable that surface-modified polymers might have sufficient mobility to exhibit similar behavior. Earlier, we described a series of contact-angle experiments that seemingly shows that the hysteresis on our surface-modified PP films is thermodynamic, rather than kinetic. That data would argue against the type of reorientation proposed by Yasuda *et al.* However, if the reorientation were nearly instantaneous, it might be difficult to experimentally detect it. Thus, it is possible that an extremely rapid reorientation of oxidized scission products could account for some of the hysteresis that we observe.

6. CONCLUSIONS

Although both corona and flame treatments of polypropylene are surface-oxidation processes, the two methods differ considerably in the mechanism of oxidation. Corona discharges are dominated by O-atom reactions that lead to scission of the PP and to the formation of water-soluble LMWOM. The LMWOM agglomerates into mounds that are plainly visible in AFM images. The extensive scission associated with corona processes affects the wettability and stability of the treated PP films. By contrast, flame surface oxidations are dominated by OH-radical reactions that lead to oxidation without LMWOM formation. The more limited chain scission associated with flame treatment leads to the formation of topographic nodules of intermediate-molecular-weight materials that are much smaller than the mounds of LMWOM. Because of the lack of LMWOM formation, flame-treated PP is more highly oxidized after washing with water, more wettable, and more stable than corona-treated PP.

The effect of increasing relative humidity in a corona is to decrease the O/OH ratio in the gas phase. This leads to less formation of LMWOM at higher RH. However, at higher humidities, any LMWOM that is formed is more likely to agglomerate because of the enhanced mobility imparted by adsorbed water vapor.

Untreated, corona-treated, and flame-treated PP all exhibit considerable thermodynamic contact-angle hysteresis. While topographic features are the likely cause of the hysteresis on untreated PP, microscopic chemical heterogeneity is the

major contributor to the hysteresis on the surface-oxidized PP. The importance of using AFM to assess surface topography is quite obvious. Without AFM images, it is impossible to determine if there is a possible effect of roughness on the contact-angle measurements of oriented polymers.

ACKNOWLEDGMENTS

REFERENCES

1. M. Strobel, M. J. Walzak, J. M. Hill, A. Lin, E. Karbashewski, and C. S. Lyons, *J. Adhes. Sci. Technol.* **9**, 365 (1995).
2. M. Strobel, C. Dunatov, J. M. Strobel, C. S. Lyons, S. J. Perron, and M. C. Morgen, *J. Adhes. Sci. Technol.* **3**, 321 (1989).
3. J. M. Strobel, M. Strobel, C. S. Lyons, C. Dunatov, and S. J. Perron, *J. Adhes. Sci. Technol.* **5**, 119 (1991).
4. M. Strobel, C. S. Lyons, J. M. Strobel, and R. S. Kapaun, *J. Adhes. Sci. and Technol.* **6**, 429 (1992).
5. M. Strobel, N. Sullivan, M. C. Branch, V. Jones, J. Park, M. Ulsh, J. M. Strobel, and C. S. Lyons, *J. Adhes. Sci. Technol.* **15**, 1 (2001).
6. T. C. Manley, *Trans. Electrochem. Soc.* **84**, 83 (1943).
7. M. C. Branch, N. Sullivan, M. Ulsh, and M. Strobel, in *Twenty-Seventh Symposium (International) on Combustion*, The Combustion Institute, Pittsburgh, PA (1998), pp. 2807.
8. M. Strobel, N. Sullivan, M. C. Branch, J. Park, M. Ulsh, R. S. Kapaun, and B. Leys, *J. Adhes. Sci. Technol.* **14**, 1243 (2000).
9. F. Garbassi, M. Morra, and E. Occhiello, *Polymer Surfaces*, Wiley, Chichester, England (1994), Ch. 4.
10. NIST Chemical Kinetics Database, version 2Q98 (1998).
11. A. C. Gentile and M. J. Kushner, *J. Appl. Phys.* **78**, 2074 (1995).
12. M. B. Chang, J. H. Balbach, M. J. Rood, and M. J. Kushner, *J. Appl. Phys.* **69**, 4409 (1991).
13. R. Dorai and M. J. Kushner, *J. Phys. D: Appl. Phys.* **34**, 574 (2001).
14. P. N. Brown, A. C. Hindmarsh, and G. D. Byrne, *Variable-Coefficient Ordinary Differential Equation Solver*, Lawrence Livermore Laboratories, Livermore, CA (1989).
15. R. M. Overney, R. Lüthi, H. Haefke, J. Frommer, E. Meyer, H.-J. Güntherodt, S. Hild, and J. Fuhrmann, *Appl. Surf. Sci.* **64**, 197 (1993).
16. G. J. Vancso, T. D. Allston, I. Chun, L.-S. Johansson, G. Liu, and P. F. Smith, *Int. J. Polym. Anal. Characteriz.* **3**, 89 (1996).
17. S. Süzer, A. Argun, O. Vatansever, and O. Aral, *J. Appl. Polym. Sci.* **74**, 1846 (1999).
18. H.-Y. Nie, M. J. Walzak, B. Berno, and N. S. McIntyre, *Appl. Surf. Sci.* **144/145**, 627 (1999).
19. H.-Y. Nie, M. J. Walzak, and N. S. McIntyre, *Polymer* **41**, 2213 (2000).
20. L.-A. O'Hare, S. Leadley, and B. Parbhoo, *Surf. Interface Anal.* **33**, 335 (2002).
21. S. Guimond, I. Radu, G. Czeremuszkin, D. J. Carlsson, and M. R. Wertheimer, *Plasmas Polym.* **7**, 71 (2002).
22. O. D. Greenwood, R. D. Boyd, J. Hopkins, and J. P. S. Badyal, *J. Adhes. Sci. Technol.* **9**, 311 (1995).

23. R. D. Boyd, A. M. Kenwright, J. P. S. Badyal, and D. Briggs, *Macromolecules* **30**, 5429 (1997).
24. G. J. Vancso, T. D. Allston, I. Chun, L.-S. Johansson, G. Liu, and P. F. Smith, *Int. J. Polym. Anal. Characteriz.* **3**, 89 (1996).
25. D. Briggs, C. R. Kendall, A. R. Blythe, and A. B. Wootton, *Polymer* **24**, 47 (1983).
26. C. Y. Kim and D. A. I. Goring, *J. Appl. Polym. Sci.* **15**, 1357 (1971).
27. R. Mahlberg, H. E.-M. Niemi, F. S. Denes, and R. M. Rowell, *Langmuir* **15**, 2985 (1999).
28. H. F. Mark (executive ed.), *Encyclopedia of Chemical Technology*, 3rd ed., Vol. 16, Wiley-Interscience, New York (1981), p. 689.
29. J. F. Rabek, *Polymer Photodegradation Mechanisms and Experimental Methods*, Chapman and Hall, London (1995), Chs. 2, 3, 6, and 7.
30. D. J. Carlsson and D. M. Wiles, *J. Macromol. Sci., – Rev. Macromol. Chem.* **C14**, 65 (1976).
31. S. J. Moss, A. M. Jolly, and B. J. Tighe, *Plasma Chem. Plasma Process.* **6**, 401 (1986).
32. F. D. Egitto, V. Vukanovic, and G. N. Taylor, Plasma Etching of Organic Polymers, in *Plasma Deposition, Treatment, and Etching of Polymers*, R. d'Agostino, ed., Academic Press, San Diego, CA (1990), p. 339.
33. R. Paltenghi, E. A. Ogryzlo, and K. D. Bates, *J. Phys. Chem.* **88**, 2595 (1984).
34. R. H. Hansen, J. V. Pascale, R. De Benedictis, and P. M. Rentzepis, *J. Polym. Sci. A* **3**, 2205 (1965).
35. A. Holländer, J. E. Klemberg-Sapieha, and M. R. Wertheimer, *Macromolecules* **27**, 2893 (1994).
36. A. C. Fozza, J. E. Klemberg-Sapieha, and M. R. Wertheimer, *Plasmas Polym.* **4**, 183 (1999).
37. L. A. Rosocha and R. A. Korzekwa, *J. Adv. Oxid. Technol.* **4**, 247 (1999).
38. O. K. Fomin, *Russ. Chem. Rev.* **36**, 725 (1967).
39. R. Brown and C. A. Winkler, *Angew. Chem. Int. Ed.* **9**, 181 (1970).
40. G. Kill, D. H. Hunter, and N. S. McIntyre, *J. Polym. Sci. A: Polym. Chem.* **34**, 2299 (1996).
41. E. M. Liston, L. Martinu, and M. R. Wertheimer, *J. Adhes. Sci. Technol.* **7**, 1091 (1993).
42. R. Foerch, G. Kill, and M. J. Walzak, *J. Adhes. Sci. Technol.* **7**, 1077 (1993).
43. G. Z. Xio, *J. Adhes. Sci. Technol.* **11**, 655 (1997).
44. M. J. Walzak, S. Flynn, R. Foerch, J. M. Hill, E. Karbashewski, A. Lin, and M. Strobel, *J. Adhes. Sci. Technol.* **9**, 1229 (1995).
45. L. F. Macmanus, M. J. Walzak, and N. S. McIntyre, *J. Polym. Sci. A: Polym. Chem.* **37**, 2489 (1999).
46. M. Morra, E. Occhiello, and F. Garbassi, *Adv. Colloid Interface Sci.* **32**, 79 (1990).
47. C.-M. Chan, *Polymer Surface Modification and Characterization*, Hanser/Gardner, Cincinnati, OH (1994), Ch. 2.
48. J. P. Youngblood and T. J. McCarthy, *Macromolecules* **32**, 6800 (1999).
49. M. Iring and F. Tudos, *Prog. Polym. Sci.* **15**, 217 (1990).
50. A. Holmström and E. Sörvik, *J. Polym. Sci., Polym. Chem. Ed.* **16**, 2555 (1978).
51. D. J. Carlsson and S. Chmela, Polymers and High-Energy Irradiation: Degradation and Stabilization, in *Mechanisms of Polymer Degradation and Stabilization*, G. Scott, ed., Elsevier Applied Science, London (1990), Ch. 4, p. 113.
52. N. S. Allen and M. Edge, *Fundamentals of Polymer Degradation and Stabilisation*, Elsevier Applied Science, London (1992), p. 14.
53. A. Holländer, J. E. Klemberg-Sapieha, and M. R. Wertheimer, *J. Polym. Sci. A: Polym. Chem.* **33**, 2013 (1995).
54. H. Yasuda, A. K. Sharma, and T. Yasuda, *J. Polym. Sci., Polym. Phys. Ed.* **19**, 1285 (1981).
55. C. W. Weikart and H. K. Yasuda, *J. Polym. Sci. A: Polym. Chem.* **38**, 3028 (2000).